Available online at http://scik.org
Commun. Math. Biol. Neurosci. 2024, 2024:82
https://doi.org/10.28919/cmbn/8665
ISSN: 2052-2541

OPTIMAL CONTROL STRATEGIES OF MULTISTRAIN INFECTIOUS DISEASE WITH LIMITED VACCINATION AND TREATMENT CAPACITY

REFI REVINA, TONI BAKHTIAR, JAHARUDDIN*

Department of Mathematics, Faculty of Mathematics and Natural Sciences, IPB University, IPB Campus Dramaga, Bogor 16680, Indonesia

Abstract. In this paper, the multistrain SVEIR model is considered which represents the evolution of susceptible, vaccinated, exposed, infected, and recovered individuals. Based on this model, the stability properties of the disease-free equilibrium is obtained. Furthermore, the model was expanded by applying optimal control theory with limited vaccination and treatment capacity presented in four strategies. We used COVID-19 a case study, based on the order of the first and second strains representing milder and more severe symptoms. Numerical results show that the fourth strategy produces endemic spike peaks that occur much lower, which means this strategy is capable and quite effective. However, based on cost effectiveness analysis using the Average Cost Effectiveness Ratio (ACER) and Incremental Cost Effectiveness Ratio (ICER) methods in decision making, the first strategy is optimal and cost effective.

Keywords: infectious disease; model's stability; multistrain SVEIR model; optimal control; strategy.

2020 AMS Subject Classification: 92D25, 34D20, 34C40.

1. INTRODUCTION

Infectious diseases arise due to disharmonious interactions between the host and infectious agents, which are microorganisms in the form of fungi, viruses, bacteria, or parasites that spread

*Corresponding author
E-mail address: jaharmath@gmail.com
Received May 28, 2024

diseases that enter the body. The results of this interaction can ultimately cause individuals to contract an infection, which can be transferred to other individuals directly or through intermediaries [1].

Infectious agents in the form of viruses are known to undergo mutations, resulting from an error when the virus reproduces and produces a virus different from the parental strain or a virus variant. When the results of a modification show evident physical characteristics and are different from the original virus, this can be called a strain [2]. Several infectious diseases are caused by more than one strain, such as influenza, Neisseria gonorrhoeae, dangue fever, and COVID-19. Until the Indonesian government revoked the status of the COVID-19 pandemic in June 2023, the last two years have devastated the fabric of social life by claiming many lives and harming various sectors, namely health, economics, social, and education globally [3].

Due to the many detrimental global impacts, infectious diseases are a significant challenge for the world community. The emergency committee states that the transmission of infectious diseases can be minimized or even stopped with several preventive measures, such as vaccination and treatment [4, 5]. The official United Nations website expalined that the global vaccine distribution process is considered to be uneven due to limited supply. Apart from that, the problem of a lack of individual awareness about vaccinating can be caused by doubts and speculation, as well as concerns about the side effects caused by vaccines [6, 7]. Only some individuals can afford vaccination, ultimately indicated by the explanation above.

Based on the situations and problems arising from the infectious diseases described above, scientists from various scientific disciplines work together to research and discuss problems to find responsive solutions to urgent situations stated by WHO disturbing the global community. To achieve this goal, the field of mathematics through mathematical modeling plays an essential role in efforts that focus on predicting, estimating, and controlling the potential for infectious diseases [8]. Mathematical modeling can provide an understanding of infectious disease transmission patterns and detection parameters to reduce infected individuals in a population [9].

This scientific work discusses the dynamics of the spread of multistrain infectious diseases using mathematical modeling explicitly. The uncontrolled multistrain SEIR model by Khyar and Allali [10] will upgrade to a model that considers controls in the form of vaccination and treatment, then we also investigate the stability of equilibrium points. Apart from that, implementing optimal control theory also plays a role in identifying optimal control strategies to minimize the number of exposed and infected individuals by considering cases of limited vaccine supplies.

This paper is organized into six parts. After the introductory section and research background in Section 1, we present in Section 2 a development of the model and assumptions. In section 3, dynamic properties are discussed which include the stability of the disease-free equilibrium point based on the basic reproduction number. In section 4, models with optimal control are discussed. Section 5 is devoted to numerical simulations. Conclusions and directions for future research are presented in Section 6.

2. MODEL FORMULATION

In this section, we introduce the multistrain SVEIR model by dividing the human population into seven classes, namely susceptible human population (S), exposed to the first strain (E_1), exposed to the second strain (E_2), infected with mild symptoms (I_1), infected with severe symptoms (I_2), recovered human population (R), and human population who are vaccinated (V). The model made was the addition of a compartment V, which represents the number of individuals who have been vaccinated (vaccinated) with parameters $u_1(t)$ as the rate of susceptible individuals who receive the first dose of vaccination, $u_2(t)$ represents the rate of vaccinated individuals who receive the second dose of vaccination, and $u_3(t)$ states the rate of treatment from individuals infected with strain two to recovery. In this model, there are several assumptions below:

1. Each individual in the population has the same probability of being infected [11].
2. Individuals who have recovered have immunity to the virus and will not return to the susceptible (S) subpopulation [12].

3. Individuals infected by strain one are not infected by strain two.
4. Individuals who have been vaccinated do not necessarily become immune to COVID-19 but only reduce symptoms when infected; therefore, there can be a transition from vaccinated (V) to subpopulations exposed to each strain (E_1 or E_2), which occurs due to interactions between individuals who have been vaccinated with infected individuals [13].
5. Due to vaccine imperfections, there is a transition from V to S within a certain period, meaning that vaccination is carried out more than once to strengthen the previously formed immune response [13].

Based on the assumptions above, the dynamics of the spread of COVID-19 can be illustrated in the compartment diagram in Figure 1.

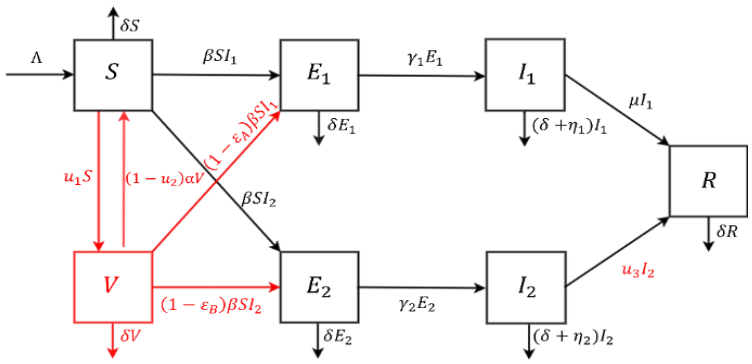

Figure 1. Multistrain SVEIR Model Compartment Diagram for COVID-19

From the schematic diagram in Figure 1, we derive the equations of motion of the model, which capture the dynamics of the spread of COVID-19. The SVEIR model can then be represented by the following set of ordinary nonlinear differential equations as follows:

$$\frac{dS}{dt} = \Lambda + (1-u_2)\alpha V - (u_1 + \beta I_1 + \beta I_2 + \delta)S,$$

$$\frac{dV}{dt} = u_1 S - ((1-u_2)\alpha + (1-\varepsilon_A)\beta I_1 + (1-\varepsilon_B)\beta I_2 + \delta)V,$$

$$\frac{dE_1}{dt} = \beta I_1 S + (1-\varepsilon_A)\beta I_1 V - (\gamma_1 + \delta)E_1,$$

$$\frac{dE_2}{dt} = \beta I_2 S + (1-\varepsilon_B)\beta I_2 V - (\gamma_2 + \delta)E_2,$$

$$\begin{aligned}\frac{dI_1}{dt} &= \gamma_1 E_1 - (\mu + \delta + \eta_1) I_1, \\ \frac{dI_2}{dt} &= \gamma_2 E_2 - (u_3 + \delta + \eta_2) I_2, \\ \frac{dR}{dt} &= \mu I_1 + u_3 I_2 - \delta R,\end{aligned} \tag{1}$$

with the initial conditions are $S(0) = S_0$, $V(0) = V_0$, $E_1(0) = E_{10}$, $E_2(0) = E_{20}$, $I_1(0) = I_{10}$, $I_2(0) = I_{20}$, $R(0) = R_0$. The description of several parameters in equation (1) is stated in Table 1.

TABLE 1. The description and numerical values for the model parameters.

Parameter	**Description**	**Values**	**Source**
Λ	Birth rate	$\frac{5000}{70 \times 365}$	Assumed
δ	Natural death rate	$\frac{5000}{70 \times 365}$	Assumed
β	COVID-19 transmission rate	0.000131	[14]
γ_1	The first strain latency rate	0.07142854	[15]
γ_2	The second strain latency rate	0.05882353	[15]
η_1	Disease-induced death rate strain 1	6.83×10^{-5}	[16]
η_2	Disease-induced death rate strain 2	6.83×10^{-5}	[16]
μ	Recovery rate for the first strain	0.15	[10]
ε_A	Vaccine effectiveness against the first strain where $0 \leq \varepsilon_A \leq 1$	0.87	[17]
ε_B	Vaccine effectiveness against the first strain where $0 \leq \varepsilon_B \leq 1$	0.87	[17]
α	The rate of decline in vaccine effectiveness after the first dose	0.5	[18]

3. DYNAMICAL PROPERTIES

In this section, we discuss the dynamical properties of the SVEIR model. We identify the existence of equilibrium points of the system and investigate their stability. We also provide the basic reproduction number of the model for analyzing the stability. System (1) has disease-free equilibrium points representing a condition that the disease, in this case the infectious disease is no longer infects the population. This results in the exposed (E_1 and E_2), infected (I_1 and I_2), and recovered (R) populations no longer existing. In the other words, this equilibrium point will contain the condition $I_1 = I_2 = 0$. The disease-free equilibrium point of the system (1) can be obtained as follows

$$T^o\ (S, V, E_1, E_2, I_1, I_2, R) = T^o\ (S^o, V^o, 0,0,0,0,0),$$

where $S^o = \frac{\Lambda}{u_1+\delta}$, and $V^o = \frac{u_1\Lambda}{\delta(u_1+\delta)}$. Using the next generation matrix method [19], the infection term and the remaining transfer terms are respectively given below:

$$\mathcal{F} = \begin{pmatrix} 0 & 0 & \frac{\beta\Lambda(u_1(1-\varepsilon_A)+\delta)}{\delta(u_1+\delta)} & 0 \\ 0 & 0 & 0 & \frac{\beta\Lambda(u_1(1-\varepsilon_B)+\delta)}{\delta(u_1+\delta)} \\ 0 & 0 & 0 & 0 \\ 0 & 0 & 0 & 0 \end{pmatrix}, \quad \mathcal{V} = \begin{pmatrix} \gamma_1+\delta & 0 & 0 & 0 \\ 0 & \gamma_2+\delta & 0 & 0 \\ -\gamma_1 & 0 & v_1 & 0 \\ 0 & -\gamma_2 & 0 & v_2 \end{pmatrix},$$

with $v_1 = \delta + \eta_1 + \mu$, and $v_2 = u_3 + \delta + \eta_2$. Next, $\mathcal{R}_0$ can be determined according to the formula $\mathcal{R}_0 = \rho(\mathcal{F}\mathcal{V}^{-1})$ where ρ called the largest non-negative or dominant eigenvalue of the product $\mathcal{F}\mathcal{V}^{-1}$. So, we obtain the basic reproduction number:

$$\mathcal{R}_0 = \max\{\mathcal{R}_0^1, \mathcal{R}_0^2\}$$

with

$$\mathcal{R}_0^1 = \frac{\beta\Lambda\gamma_1((1-\varepsilon_A)u_1+\delta)}{\delta(u_1+\delta)(\gamma_1+\delta)(\delta+\eta_1+\mu)} \text{ and } \mathcal{R}_0^2 = \frac{\beta\Lambda\gamma_2((1-\varepsilon_B)u_1+\delta)}{\delta(u_1+\delta)(\gamma_2+\delta)(u_3+\delta+\eta_2)}.$$

The basic reproduction number can be interpreted as the average number of susceptible individuals infected directly by other infected individuals and enter a still entirely susceptible

subpopulation. This number is symbolized by $\mathcal{R}_0$, which functions as a parameter to determine a disease's spread level.

Theorem 1. The disease-free equilibrium point T^0 is locally asymptotically stable when it satisfies $\mathcal{R}_0 < 1$.

Proof. Stability analysis of the disease-free equilibrium point for multistrain SVEIR model will be carried out by substituting the equilibrium point T^0 into the Jacobian matrix, so that we obtain J_{T_0}

$$J_{T_0} = \begin{pmatrix} J_{T_0}11 & 0 & 0 & 0 & J_{T_0}15 & J_{T_0}16 & 0 \\ J_{T_0}21 & J_{T_0}22 & 0 & 0 & J_{T_0}25 & J_{T_0}26 & 0 \\ 0 & 0 & J_{T_0}33 & 0 & J_{T_0}35 & 0 & 0 \\ 0 & 0 & 0 & J_{T_0}44 & 0 & J_{T_0}46 & 0 \\ 0 & 0 & J_{T_0}53 & 0 & J_{T_0}55 & 0 & 0 \\ 0 & 0 & 0 & J_{T_0}64 & 0 & J_{T_0}66 & 0 \\ 0 & 0 & 0 & 0 & J_{T_0}75 & J_{T_0}76 & J_{T_0}77 \end{pmatrix}, \quad (2)$$

with the following: $J_{T_0}11 = -u_1 - \delta, J_{T_0}15 = -\frac{\beta\Lambda}{u_1+\delta}, J_{T_0}16 = -\frac{\beta\Lambda}{u_1+\delta}, J_{T_0}21 = u_1, J_{T_0}22 = -\delta,$

$J_{T_0}25 = -\frac{\beta\Lambda u_1(1-\varepsilon_A)}{\delta(u_1+\delta)}, J_{T_0}26 = -\frac{\beta\Lambda u_1(1-\varepsilon_B)}{\delta(u_1+\delta)}, J_{T_0}33 = -\gamma_1 - \delta, J_{T_0}35 = \frac{\beta\Lambda(u_1(1-\varepsilon_A)+\delta)}{\delta(u_1+\delta)}, J_{T_0}44 =$

$-\gamma_2 - \delta, J_{T_0}46 = \frac{\beta\Lambda(u_1(1-\varepsilon_B)+\delta)}{\delta(u_1+\delta)}, J_{T_0}53 = \gamma_1, J_{T_0}55 = -\delta - \eta_1 - \mu, J_{T_0}64 = \gamma_2.$

The eigenvalues of the matrix J_{T_0} can be obtained by applying the following formula $|\lambda I - J_{T_0}| = 0$. Next, we will obtain the characteristic equation from the above operations to investigate the following eigenvalues:

$$\lambda_1 = J_{T_0}11 = -u_1 -; \lambda_2 = J_{T_0}22 = -\delta; \lambda_3 = J_{T_0}77 = -\delta.$$

Furthermore, it can be concluded that $\lambda_1, \lambda_2, \lambda_3 < 0$ because all parameters are positive. We determine $\lambda_4, \lambda_5, \lambda_6,$ and $\lambda_7$with the Routh-Hurwitz Criterion [20] by the characteristic equation below

$$\lambda^4 + a_1\lambda^3 + a_2\lambda^2 + a_3\lambda + a_4 = 0,$$

where

$$a_1 = (u_3 + \eta_2 + \gamma_2 + 2\delta) + (\mu + \eta_1 + \gamma_1 + 2\delta\ ),$$

$$a_2 = (\mu + \eta_1 + \gamma_1 + 2\delta\ )(u_3 + \eta_2 + \gamma_2 + 2\delta) + (\gamma_1 + \delta)(\delta + \eta_1 + \mu)(1 - \mathcal{R}_0^1)$$
$$+(\gamma_2 + \delta)(\delta + \eta_2 + u_3)(1 - \mathcal{R}_0^2),$$
$$a_3 = (\gamma_1 + \delta)(\delta + \eta_1 + \mu)(u_3 + \eta_2 + \gamma_2 + 2\delta)(1 - \mathcal{R}_0^1) + (\gamma_2 + \delta)(\delta + \eta_2 + u_3)$$
$$(\mu + \eta_1 + \gamma_1 + 2\delta)(1 - \mathcal{R}_0^2),$$
$$a_4 = (\gamma_1 + \delta)(\delta + \eta_1 + \mu)(\gamma_2 + \delta) + (u_3 + \delta + \eta_2)(1 - \mathcal{R}_0^1)(1 - \mathcal{R}_0^2).$$

Based on the conditions of the Routh-Hurwitz Criterion in determining the stability of disease-free equilibrium point when $R_0^1 < 1$ and $\mathcal{R}_0^2 < 1$, the following conditions are satisfying: (i) $a_1, a_2, a_3, a_4 > 0$. (ii) $a_1 a_2 - a_3 > 0$. (iii) $a_1 a_2 a_3 - a_1^2 a_4 - a_3^2 > 0$. This proof concludes that the disease-free equilibrium point T^0 is locally asymptotically stable. ■

4. OPTIMAL CONTROL ANALYSIS

In previous sections, we describe the dynamics of infectious disease transmission on a multistrain SVEIR model. Thus, we investigate the optimization problem that aims to minimize the exposed subpopulation (E_1 and E_2) and infected subpopulation (I_1 dan I_2) with a minimum cost function [21]. The controls applied to this problem are vaccination and treatment. The cost function will be a nonlinear model, while the control function that will be chosen is the quadratic function u_i^2 $(i = 1, 2, 3)$. The objective function for the model with control in this research will be defined in the following form:

$$\min J(u) = \int_{t_0}^{T} \left(C_1 E_1 + C_2 E_2 + C_3 I_1 + C_4 I_2 + \frac{1}{2} \sum_{i=1}^{3} B_i u_i^2 \right) dt, \tag{3}$$

where t_0 is the initial time, T represents the final time, B_1 represents the cost weight for the first dose of vaccination, B_2 represents the cost weight for the second dose of vaccination, so B_3 represents the cost weight for treatment, and C_j $(j = 1, 2, 3, 4)$ is the positive weight to showing the relative importance among for each E_1, E_2, I_1, and I_2. System (1) is constraint for equation (3) and we want to get the control for this problem with the form $u^* = [u_1^*, u_2^*, u_3^*]^T$, such that:

$$J(u^*) = \min J(u). \tag{4}$$

The optimal control u_i will be dynamic and can change over time due to selecting the best control rate to produce the maximum performance index and system settings (1) from a fixed initial to a free terminal time state below

$$S(T), V(T), E_1(T), E_2(T), I_1(T), I_2(T), R(T) \text{ are free.} \tag{5}$$

Furthermore, the Hamiltonian function formulated below for the necessary conditions for optimality using the Pontryagin's maximum principle. For the underlying control problem, the Hamiltonian $\mathcal{H}$ is given on equation (6) below

$$\mathcal{H} = C_1E_1 + C_2E_2 + C_3I_1 + C_4I_2 + \frac{1}{2}[B_1u_1^2 + B_2u_2^2 + B_3u_3^2] + \sum_{i=1}^{7} p_iA_i, \tag{6}$$

with $p_i \neq 0$ called adjoint of time t corresponding to state variable or Lagrange multipliers, then A_i is the right-hand side of system (1). In dynamic optimization problems, p_i as the adjoint function is the shadow price (the marginal value of the vector or state variable x) that shows the performance index (3) rate of change (increase/decrease). The optimality conditions for the problems in the function above can be obtained by fulfilling the necessary condition for optimality following Pontryagin's maximum principle below

$$\frac{\partial \mathcal{H}}{\partial u_i} = 0; \quad i = 1, 2, 3, \tag{7}$$

$$\dot{x_j}(t) = \frac{\partial \mathcal{H}}{\partial p}; \; j = 1, 2, \dots, 7; \; x \in \{S, V, E_1, E_2, I_1, I_2, R\}, \tag{8}$$

$$\dot{p_j}(t) = -\frac{\partial \mathcal{H}}{\partial x}; \; j = 1, 2, \dots, 7; \; x \in \{S, V, E_1, E_2, I_1, I_2, R\}. \tag{9}$$

We called (7) as the optimal control of this problem, corresponding to (8), which found in the equation of the multistrain SVEIR model itself, and (9) produced an adjoint system. The optimal control u_1^*, u_2^*, and u_3^* that satisfy (7) are given by

$$\boldsymbol{u_1^* = \min\left\{u_{1_{max}}, \max\left(0, \frac{S(p_1 - p_2)}{B_1}\right)\right\}}, \tag{10}$$

$$u_2^* = \min\left\{u_{2_{max}}, \max\left(0, \frac{\alpha V(p_1 - p_2)}{B_2}\right)\right\}, \tag{11}$$

$$u_3^* = \min\left\{u_{3_{max}}, \max\left(0, \frac{I_2(p_6 - p_7)}{B_3}\right)\right\}. \tag{12}$$

Each control variables has the following boundary $0.001 \le u_1 \le u_{1_{max}} \le 0.15,\ 0 \le u_2 \le u_{2_{max}} \le 0.009$, and $0 \le u_3 \le u_{3_{max}} \le 0.05$.). It means that if $u_i < 0$ for some interval of t, then we set the value of $u_i = 0$ in that interval. Similarly, if u_i is greater than the upper bound of each control, then $u_i = 1$ for some t. These expressions will be beneficial when determining a numerical solution for the problem. By (*7*) there exists u_1^*, u_2^*, and u_3^* and corresponding optimal state $\dot{S}, \dot{V}, \dot{E_1}, \dot{E_2}, \dot{I_1}, \dot{I_2}$, and $\dot{R}$ by (8) that satisfies (4). Furthermore, there exist adjoint functions p_j $(j = 1, 2, \dots, 7)$ by (9), such that:

$$\begin{aligned}
\dot{p_1} &= -\frac{\partial \mathcal{H}}{\partial S} = p_1(u_1 + \beta I_1 + \beta I_2 + \delta) - p_2 u_1 - p_3\,\beta I_1 - p_4\,\beta I_2,\\
\dot{p_2} &= -\frac{\partial \mathcal{H}}{\partial V} = -p_1(1-u_2)\alpha + p_2[(1-u_2)\alpha + (1-\varepsilon_A)\beta I_1 + (1-\varepsilon_B)\beta I_2 + \delta)]\\
&\quad - p_3(1-\varepsilon_A)\beta I_1,\\
\dot{p_3} &= -\frac{\partial \mathcal{H}}{\partial E_1} = -C_1 + p_3[\gamma_1 + \delta] - p_5\gamma_1,\\
\dot{p_4} &= -\frac{\partial \mathcal{H}}{\partial E_2} = -C_2 + p_4[\gamma_2 + \delta] - p_6\gamma_2,\\
\dot{p_5} &= -\frac{\partial \mathcal{H}}{\partial I_1} = -C_3 + p_1 S\beta + p_2(1-\varepsilon_A)\beta V - p_3(\beta S + \beta V(1-\varepsilon_A)) + p_5[\mu + \delta\\
&\quad + \eta_1] - p_7\mu,\\
\dot{p_6} &= -\frac{\partial \mathcal{H}}{\partial I_2} = -C_4 + p_1\beta S + p_2(1-\varepsilon_B)\beta V - p_4(\beta S + \beta V(1-\varepsilon_B))\\
&\quad + p_6[u_3 + \delta + \eta_2] - p_7 u_3,\\
\dot{p_7} &= -\frac{\partial \mathcal{H}}{\partial R} = p_7\delta.
\end{aligned} \tag{13}$$

The transversality condition should be fulfilled below,

$$p_j(T) = 0; j = 1, 2, \dots, 7. \tag{14}$$

5. NUMERICAL SIMULATIONS

5.1.The Dynamic of Model with Constant Control

The stability of equation (1) and the effectiveness of the strategy can be verified by carrying out numerical simulations with the following initial values for each population $S(0) = 4825, V(0) = 150, E_1(0) = 9, E_2(0) = 6, I_1(0) = 4, I_2(0) = 5$, and $R(0) = 1$. Considering the parameters on the Table 1, the following is a numerical simulation for the model with constant control and a model with optimum control.

Numerical solutions have been obtained in the form of graphs for the dynamics of each subpopulation for endemic conditions by considering the parameters in Table 1 and the initial values of the subpopulations for the respective models explained above. Thus, simulations of the multistrain SVEIR model will also consider variations in constant control parameters for vaccination rates with a rate of 0.06 and treatment with rates of 0.1 and 0.05.

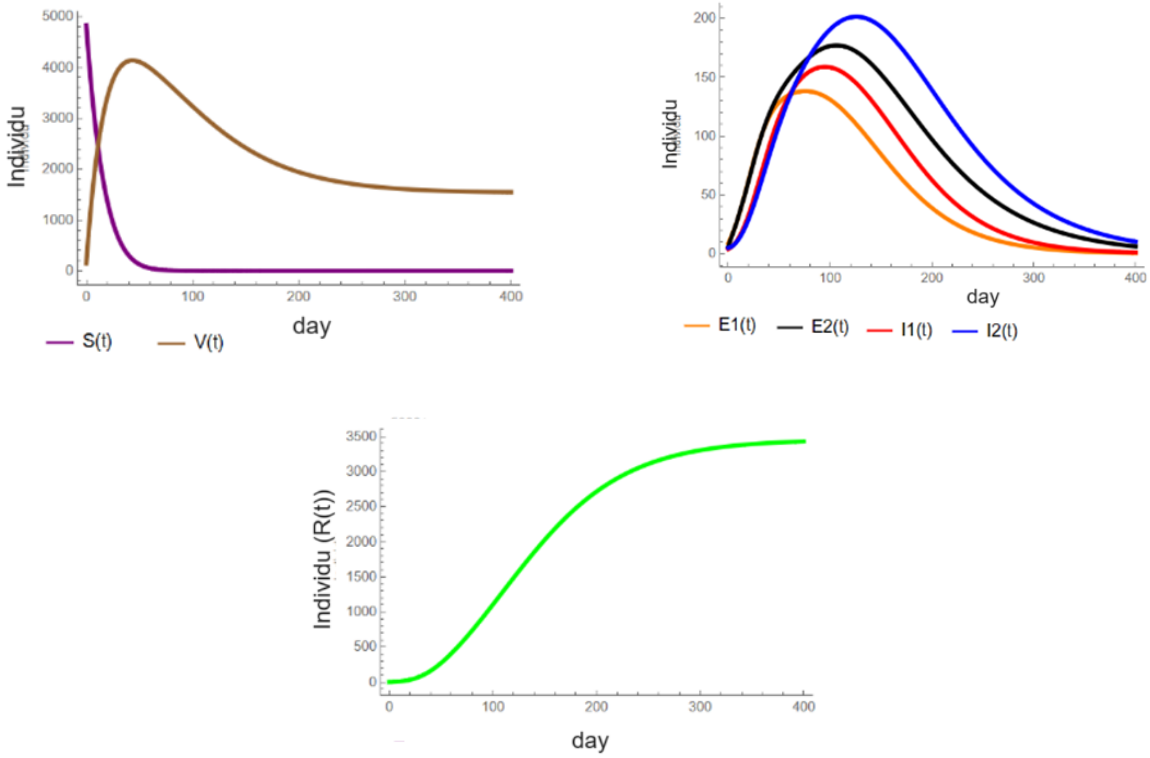

FIGURE 2. The dynamics of population for Model with constant control when $\mathcal{R}_0 = 1.7056 >$ 1.

Based on the graph above illustrate that the susceptible subpopulation decreased over time and then stabilized towards its equilibrium point. The vaccinated subpopulation experienced an increase from the initial value and then decreased until it reached the equilibrium point. The exposed (E_1 and E_2) and infected (I_1 and I_2) subpopulations experienced an increase from the initial value. These four subpopulations reached the endemic peak and decreased over time, then appeared to stabilize towards their respective equilibrium points.

5.2.The Dynamic of Model with Optimal Control

In this section, we discuss the numerical simulation results of the multistrain SVEIR model by applying optimal control. In this simulation, we assume that $B_1 = 30$, $B_2 = 20$, $C_1 = 1$, $C_2 = 2$, $C_3 = 1$, and $C_4 = 2$. This problem numerically solved by well-known The 4th Order Runge-Kutta then we combine it with the Forward-Backward Sweep Method. This problem has four strategies with three control instruments listed in Table 2.

TABLE 2**.** Control Strategies.

	u_1	u_2	u_3
Constant Control	0.001	0.0005	0.003
1st Strategy	$[0.001, 0.006]$	0	$[0.001, 0.05]$
2nd Strategy	$[0.001, 0.01]$	$[0, 0.007]$	$[0.001, 0.05]$
3rd Strategy	$[0.001, 0.09]$	$[0, 0.03]$	$[0.001, 0.05]$
4th Strategy	$[0.001, 0.15]$	$[0, 0.09]$	$[0.001, 0.05]$

The dynamics of S, V, E_1, E_2, I_1, I_2, and R in the model with optimal control by considering the intervals of each control u_1, u_2, and u_3 for 400 days are illustrated in Figure 3.

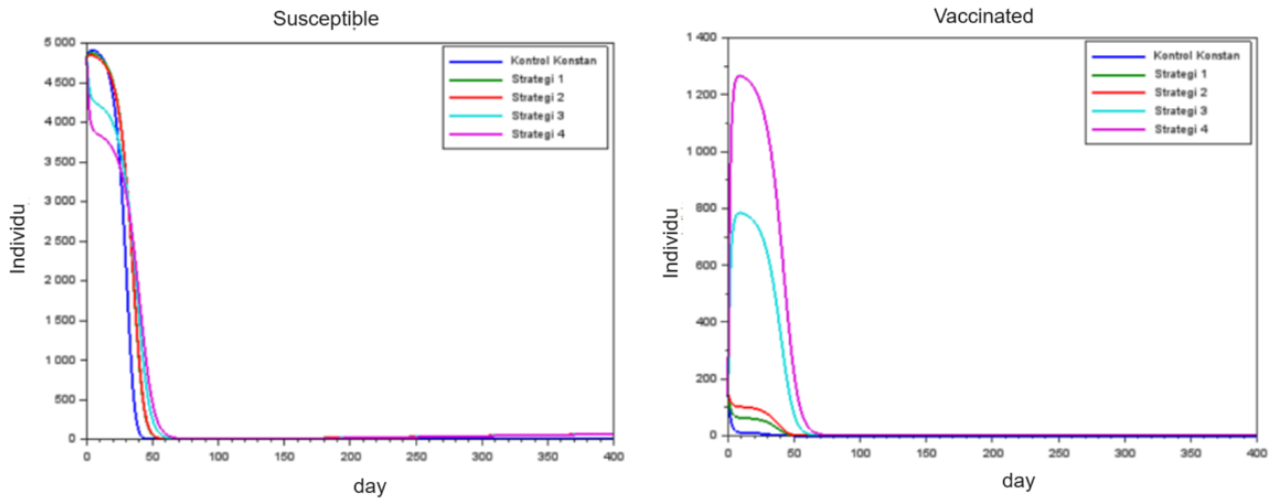

FIGURE 3. The dynamics of S and V subpopulation for mathematical model with optimal control

Figure 3 illustrate the size of the S subpopulation for 400 days. The first and second strategies shows a slight increase from the initial value and require a longer time than constant control, third strategy, and fourth strategy for the S subpopulation to experience a decline. Meanwhile, constant control experienced an increase and was assessed as requiring a longer time to experience a significant decrease compared to the fourth and third strategies. However, there was a very significant decrease compared to other strategies the following day. Based on the graph, the fourth strategy is an effective strategy to reduce the S subpopulation.

For the vaccinated subpopulation, the fourth strategy, there has been an increase in subpopulation V. Providing complete vaccination in the third strategy is also considered quite good in increasing the size of subpopulation V. As for constant control. The first and second strategies have also increased but not significantly compared to the third and fourth strategies. Therefore, the fourth strategy is the most effective for increasing subpopulation V.

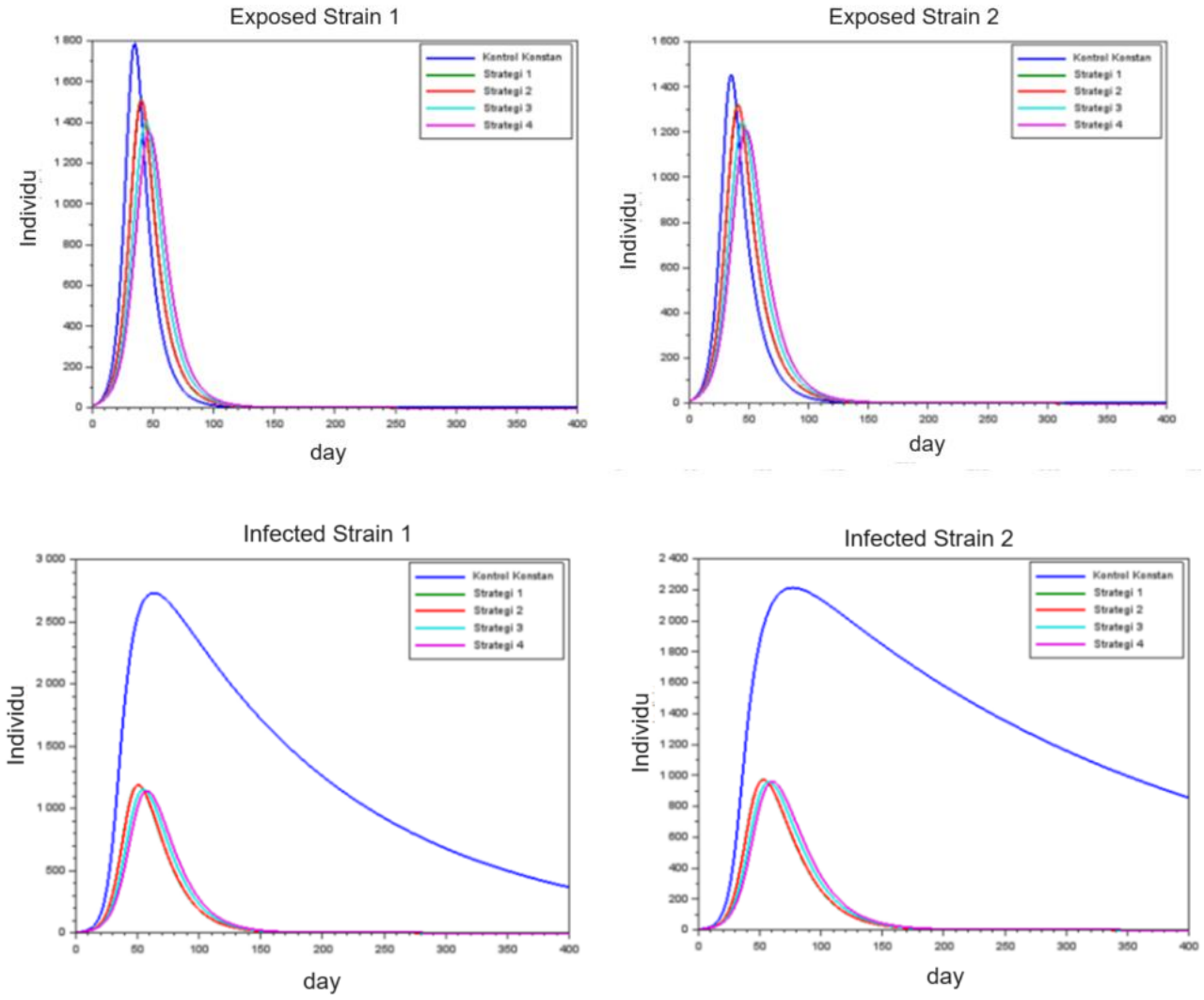

FIGURE 4. The dynamics of E_1, E_2, I_1, and I_2 subpopulation for mathematical model with optimal control

Figure 4 illustrate that the application of optimal control affects controlling COVID-19. Modeling with constant control applies the same control from initial to final conditions and, if displayed on a graph, will form a constant function. In this case, the application of constant control tends to increase towards a higher and faster endemic peak when compared to models that apply optimal control to the other four strategies. Modeling with the application of optimal control has a dynamic control form where each control function will choose the optimal rate or, in this case, what control rate (u_1^*, u_2^*, and u_3^*) is best and has optimal results. The graphs in

Figure 4 show that the fourth strategy is the most effective in reducing the number and delaying the spike in cases from the exposed and infected subpopulations for both strains.

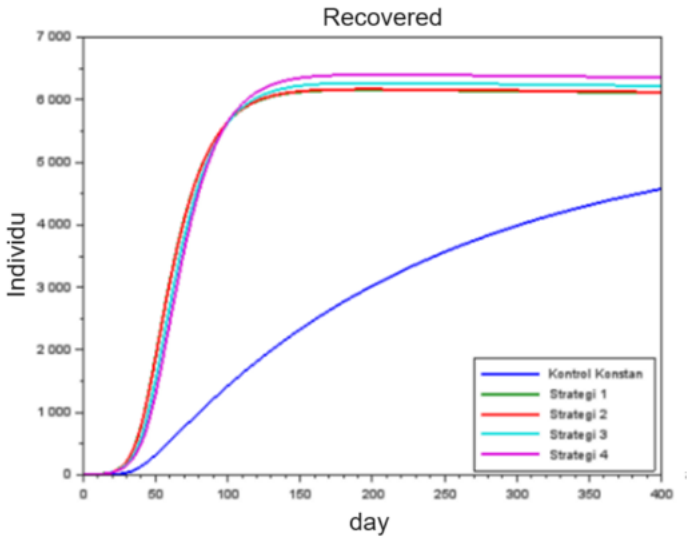

FIGURE 5. The dynamics of *R* subpopulation for mathematical model with optimal control

Figure 5 shows the *R* subpopulation increases over time due to the movement of other recovered subpopulations. The fourth strategy has a higher number of recoveries when compared to others.

One of the main objectives of this study is to find strategies that have optimal results for minimizing the performance index (J) under four different intervention strategies.

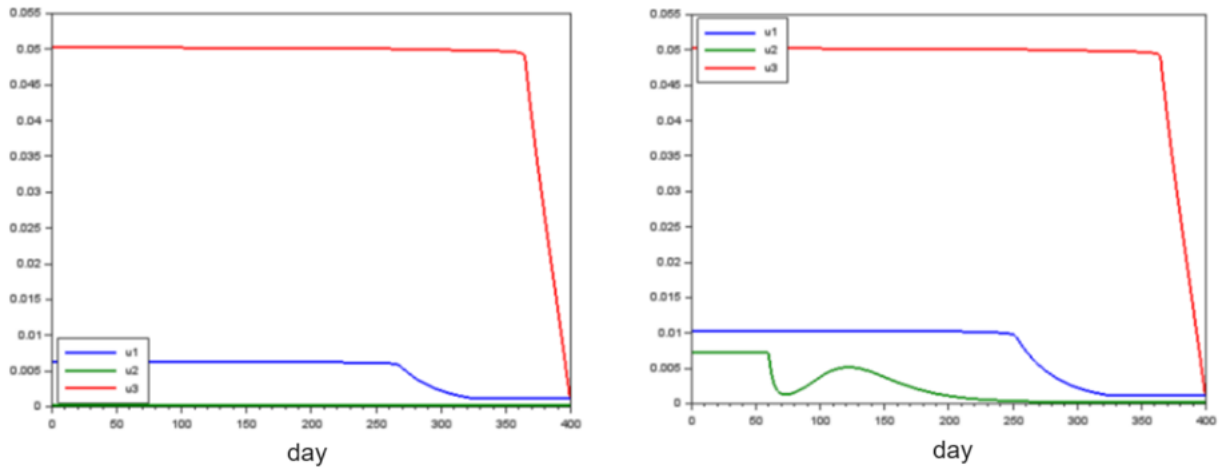

(a) 1st strategy (b) 2nd strategy

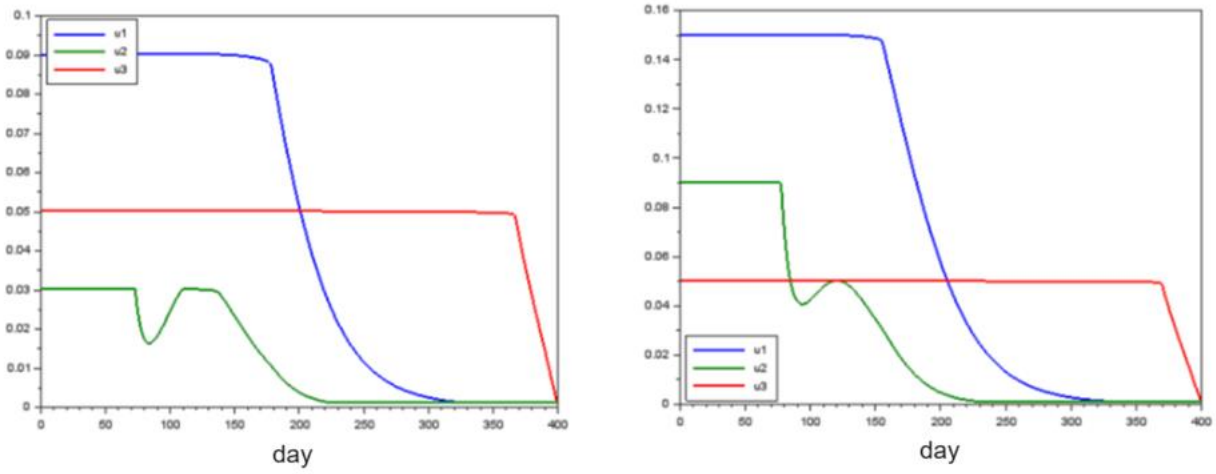

(c) 3rd strategy (d) 4th strategy

FIGURE 6. Graph of four control strategies for 400 days

Figure 6 illustrate whenever applicable, treatment should be fully applied almost all the time. It indicates the importance of the treatment even then the effectiveness of the control strategy is relatively low. Figure 6(a) shows that in the 1st strategy, a maximum effort is made to vaccinate the first dose for 270 days and treatment at a maximum rate per day of 0.05 of the population for 365. In 2nd strategy in Figure 6(b), control is carried out at a maximum rate for the first vaccination dose for 250 days, the second dose for 60 days, and the maximum treatment rate for 365 days. Furthermore, in Figure 6(c), it can be seen that the first vaccination was implemented maximally for 180 days, the second vaccination of 0.03 of the total population in units per day was carried out for 60 days, the maximum treatment was carried out within 370 days, and after the application of the rate in total maximum in each control after which the rate can be reduced. The fourth strategy in Figure 6(d) shows the implementation of control in the form of first-dose vaccination, second-dose vaccination, and maximum treatment sequentially for 160 days, 80 days, and 370 days.

5.3.Cost-effectiveness Analysis

Cost-effectiveness analysis is an analysis technique in the economic realm that compares two or more options available for health interventions by considering the ratio of the difference in costs and outcomes of each option. In simple terms, cost-effectiveness analysis is carried out to

assist in decision-making and policies so that the option with the best cost-effectiveness is selected, especially in the health domain [22, 23]. In this cost-effectiveness analysis, *Average Cost Effectiveness Ratio* (ACER) and *Incremental Cost Effectiveness Ratio* (ICER) were implemented. ACER represents the average cost used per unit of health benefit. ICER shows the determination of additional costs that must be incurred per unit. This section will bring us to the best strategy with optimal result and cost-effective with the following formula:

$$\text{ACER}\ (j) = \frac{\text{Total cost of intervention}}{\text{The number of infections avoided}}$$

where the total cost of the intervention can be determined by calculating

$$W_j = \int_0^T \frac{1}{2}\left(B_1 u_{1,j}^2 + B_2 u_{2,j}^2 + B_3 u_{3,j}^2\right) dt.$$

$u_1, u_2,$ and u_3 are the optimal control for T period and obtained in j^{th} strategy with $j = 1,2,3,4$. Then, the total number of infections avoided calculated as

$$M_j = Z^j(T) - Z(T),$$

where $Z^j(T) = \int_0^T E_{1,j} + E_{2,j} + I_{1,j} + I_{2,j}\, dt$ for each strategy and $Z(T)$ is the number of infections with no control. ICER calculated as

$$ICER(j) = \frac{W_{j+1} - W_j}{M_{j+1} - M_j}.$$

For this work, we got the result of ACER and ICER for this problem in Table 3.

TABLE 3. Calculation of ACER and ICER.

Strategy	*Benefit*	Cost	ACER	ICER
4th Strategy	135197.54	66.551592	0.0004923	D
3rd Strategy	139731.87	21.410577	0.0001532	D
2nd Strategy	144645.23	1.3317139	0.0000092	D
1st Strategy	144846.31	1.1013760	0.0000076	0.0000076

Based on the identification results above, the first strategy is considered the most cost-effective.

6. CONCLUSION

This multistrain SVEIR model has disease-free and endemic equilibrium points. Analysis of the stability of disease-free equilibrium points and endemic equilibrium points carried out for research data can be considered locally asymptotically stable.

Numerical simulations were carried out on four control strategies. The simulation graphs obtained were then analyzed to determine the effect of the four control strategies. The application of optimal control in the four strategies is considered to provide a positive response to suppress exposed and infected individuals compared to the application of constant control. By numerical simulations, the fourth strategy is considered the best to be implemented to suppress exposed and infected subpopulations. However, according to the cost-effectiveness analysis, it was found that the first strategy was cost-effective with optimal results.

As the booster vaccine has been developed, the future researchers will be able to involve the rate of the first and second booster vaccinations as well as being equipped with a sensitivity analysis of vaccination and considering the vaccination capacity at the interval (0, M] with M being the number of susceptible populations who can be vaccinated up to time T based on estimates of public awareness or WHO targets, thereby implementing optimal control problems with integral constraints or what are known as isoperimetric constraints.

ACKNOWLEDGEMENT

This work is fully supported by the Ministry of Education, Culture, Research, and Technology of Indonesia (Kemendikbudristek RI) through the Master's Thesis Research Scheme. The authors also gratefully acknowledge the helpful comments and suggestions of the reviewers, which have improved the presentation.

CONFLICT OF INTERESTS

The authors declare that there is no conflict of interests.

REFERENCES

[1] A.S. Fauci, D.M. Morens, The perpetual challenge of infectious diseases, N. Engl. J. Med. 366 (2012), 454–461. https://doi.org/10.1056/nejmra1108296.

[2] S.N. Rayhan, T. Bakhtiar, Jaharuddin, Two-strain tuberculosis transmission model under three control strategies, IOP Conf. Ser.: Earth Environ. Sci. 58 (2017), 012025. https://doi.org/10.1088/1755-1315/58/1/012025.

[3] N.I. Nii-Trebi, Emerging and neglected infectious diseases: insights, advances, and challenges, BioMed Res. Int. 2017 (2017), 5245021. https://doi.org/10.1155/2017/5245021.

[4] D. Athina, T. Bakhtiar, Jaharuddin, Optimal control of malaria transmission using insecticide treated nets and spraying, IOP Conf. Ser.: Earth Environ. Sci. 58 (2017), 012027. https://doi.org/10.1088/1755-1315/58/1/012027.

[5] J.M. Qu, B. Cao, R.C. Chen, COVID-19: The essentials of prevention and treatment, Elsevier, 2020.

[6] W. Arumsari, R.T. Desty, W.E.G. Kusumo, Gambaran penerimaan vaksin COVID-19 di kota semarang, Indones. J. Health Community, 2 (2021), 35-45. https://doi.org/10.31331/ijheco.v2i1.1682.

[7] A. Puspasari, A. Achadi, Pendekatan health belief model untuk menganalisis penerimaan vaksinasi COVID-19 di Indonesia, Syntax Literate: J. Ilm. Indonesia, 6 (2021), 3709-3721.

[8] C.I. Siettos, L. Russo, Mathematical modeling of infectious disease dynamics, Virulence 4 (2013), 295–306. https://doi.org/10.4161/viru.24041.

[9] A. Huppert, G. Katriel, Mathematical modelling and prediction in infectious disease epidemiology, Clin. Microbiol. Infect. 19 (2013), 999–1005. https://doi.org/10.1111/1469-0691.12308.

[10] O. Khyar, K. Allali, Global dynamics of a multi-strain SEIR epidemic model with general incidence rates: application to COVID-19 pandemic, Nonlinear Dyn. 102 (2020), 489–509. https://doi.org/10.1007/s11071-020-05929-4.

[11] A. Gumel, S. Lenhart, eds., Modeling paradigms and analysis of disease transmission models, American Mathematical Society, Providence, Rhode Island, 2010. https://doi.org/10.1090/dimacs/075.

[12] I. Cooper, A. Mondal, C.G. Antonopoulos, A SIR model assumption for the spread of COVID-19 in different communities, Chaos Solitons Fractals 139 (2020), 110057. https://doi.org/10.1016/j.chaos.2020.110057.

[13] M.A. Acuña-Zegarra, S. Díaz-Infante, D. Baca-Carrasco, et al. COVID-19 optimal vaccination policies: A modeling study on efficacy, natural and vaccine-induced immunity responses, Math. Biosci. 337 (2021), 108614. https://doi.org/10.1016/j.mbs.2021.108614.

[14] T. Li, Y. Guo, Modeling and optimal control of mutated COVID-19 (Delta strain) with imperfect vaccination, Chaos Solitons Fractals 156 (2022), 111825. https://doi.org/10.1016/j.chaos.2022.111825.

[15] M. Rabiu, R. Willie, N. Parumasur, Mathematical analysis of a disease-resistant model with imperfect vaccine,

quarantine and treatment, Ricerche Mat. 69 (2020), 603–627. https://doi.org/10.1007/s11587-020-00496-7.

[16] S.M. Garba, J.M.S. Lubuma, B. Tsanou, Modeling the transmission dynamics of the COVID-19 Pandemic in South Africa, Math. Biosci. 328 (2020), 108441. https://doi.org/10.1016/j.mbs.2020.108441.

[17] T. Pilishvili, K.E. Fleming-Dutra, J.L. Farrar, et al. Interim estimates of vaccine effectiveness of Pfizer-BioNTech and moderna COVID-19 vaccines among health care personnel — 33 U.S. sites, January–March 2021, MMWR Morb. Mortal. Wkly. Rep. 70 (2021), 753–758. https://doi.org/10.15585/mmwr.mm7020e2.

[18] X. Liu, Y. Ding, Stability and numerical simulations of a new SVIR model with two delays on COVID-19 booster vaccination, Mathematics 10 (2022), 1772. https://doi.org/10.3390/math10101772.

[19] J. Giesecke, Modern infectious disease epidemiology, CRC Press, 2017.

[20] L. Edelstein-Keshet, Mathematical models in biology, SIAM, 2005. https://doi.org/10.1137/1.9780898719147.

[21] Jaharuddin, T. Bakhtiar, Control policy mix in measles transmission dynamics using vaccination, therapy, and treatment, Int. J. Math. Math. Sci. 2020 (2020), 1561569. https://doi.org/10.1155/2020/1561569.

[22] J.L. Bootman, R.J. Townsend, W.F. McGhan, Principles of pharmaeconomics, Harvey Whitney, Cincinnatti, 1996.

[23] N. Marpaung, T. Bakhtiar, Jaharuddin, Cost-effective optimal control analysis to co-infection model of dengue fever and typhoid fever, Int. J. Ecol. Econ. Stat. 42 (2021), 42–70.